Characterization of the magnetization reversal of perpendicular Nanomagnetic Logic clocked in the ns-range

Grazvydas Ziemys, , Christian Trummer, , Stephan Breitkreutz-v. Gamm, , Irina Eichwald, , Doris Schmitt-Landsiedel, and , and Markus Becherer

Citation: AIP Advances **6**, 056404 (2016); doi: 10.1063/1.4944336
View online: http://dx.doi.org/10.1063/1.4944336
View Table of Contents: http://aip.scitation.org/toc/adv/6/5
Published by the American Institute of Physics

Characterization of the magnetization reversal of perpendicular Nanomagnetic Logic clocked in the ns-range

Grazvydas Ziemys, Christian Trummer, Stephan Breitkreutz-v. Gamm, Irina Eichwald, Doris Schmitt-Landsiedel, and Markus Becherer[a]
Institute for Technical Electronics, Technical University of Munich (TUM), Germany

(Presented 14 January 2016; received 7 November 2015; accepted 6 January 2016; published online 11 March 2016)

We have investigated the magnetization reversal of fabricated Co/Pt nanomagnets with perpendicular anisotropy within a wide range of magnetic field pulse widths. This experiment covers the pulse lengths from 700 ms to 20 ns. We observed that the commonly used Arrhenius model fits very well the experimental data with a single parameter set for pulse times above 100 ns ($t_p > 100$ ns). However, below 100 ns ($t_p < 100$ ns), a steep increase of the switching field amplitude is observed and the deviation from the Arrhenius model becomes unacceptable. For short pulse times the model can be adjusted by the reversal time term for the dynamic switching field which is only dependent on the pulse amplitude and not on temperature anymore. Precise modeling of the magnetization reversal in the sub-100 ns-range is crucially important to ensure reliable operation in the favored GHz-range as well as to explore and design new kinds of Nanomagnetic Logic circuits and architectures. [http://dx.doi.org/10.1063/1.4944336]

I. INTRODUCTION

For many decades the end of the CMOS scaling era was forecasted but until last year the CMOS industry was able to follow Moore's law quite accurately. As the size of a single transistor shrinks to several tens of atoms' the continued scaling becomes even more challenging and cost-intensive. This can be observed in the slow down of commercially introduced technology nodes during recent years.[1] There are several new approaches being followed by both industry and academia. Most of those are outlined in the Emerging Research Devices (ERD) chapter of International road map for Semiconductors (ITRS).[2] There are the three approaches foreseen for the future of electronics : "More Moore", "More than Moore"and "Beyond CMOS".[3] The first approach argues for more scaling and further increase of transistor density on the chip, the second one suggests that some of new technologies combined with CMOS on one single chip could be a solution for overcoming the problem of further increase of computing power and at the same time not causing the development and manufacturing costs to skyrocket. The last of the three approaches is "Beyond CMOS", which deals with completely new device and computing paradigms. One promising "Beyond CMOS" technology listed in ITRS is Nanomagnetic Logic with perpendicular anisotropy (pNML). In many cases there are no strict border lines between the three approaches. The same is valid with pNML, which can also be considered as "More than Moore" technology in many cases. pNML could offer several advantages over the well established CMOS. First, due to its ferromagnetic nature pNML combines logic and memory in the same technology.[4] The magnetic switching is an ultra low power process and it takes just few atto-Joules[5] to change the magnetization state of a nano-scale sized magnet. Furthermore, pNML offers irradiation hardness. Logic states are represented by the bistable magnetization perpendicular to the plane of a nanomagnet, whereas

[a]g.ziemys@tum.de

logic operations are carried out by the magnetic field coupling. The 3D nature of the magnetic stray field allows to situate the magnets in all three directions without any interconnections. This is a great advantage over CMOS where the metalization layers for contacting and interconnecting transistors hardly scale and more than ten of such layers are required in a state-of-the-art CMOS processor.[6] The feasibility of 3D monolithic integration of pNML has been demonstrated experimentally in recent years. Beside the magnetic via which allows signal routing between the different functional layers[7] in all three dimensions also the computing in 3D was proven by a fully functional manufactured 3D majority logic gate.[8] The ability to avoid interconnections and 3D stacking of functional layers allows ultra-large scale integration of logic devices on a single die.

II. PRINCIPLES OF PNML

The pNML is based on field-coupled bistable nano scaled magnets. The only two possible states (up or down perpendicular to the magnet surface) of the magnetization vector represents the binary logic states "0"and "1". The most basic component is an inverter, which comprises two magnets. The majority gates realized in 2D planar technology[9] and 3D monolithic integrated majority gates[8] have been proven to be able to execute NAND or NOR logic operations depending on one programmable input state. Using the above described devices it becomes possible to implement every logical function.

Power for the state reversal of nanomagnets, information propagation and signal processing is provided globally on the whole chip by a power clock.[5] The power clock is an oscillatory magnetic field, consisting of alternating positive and negative magnetic field pulses. The power clock is generated by an on-chip inductor and is parametrized depending on the logical functionality of the chip.[5,10]

There are several approaches to implement perpendicular magnetization for the nanomagnets. Various materials such as Co/Ni,[11] CoFeB,[12] and others were shown to provide PMA. The most common material system for pNML is ultra-thin film Co/Pt multilayers. Co/Pt films stacked to several multilayers provide high net magnetic saturation. Furthermore, this material system is robust, however, due to its high intrinsic switching field, alternative materials need to be investigated and optimized for pNML to provide both low switching field and high magnetic saturation. Low coercivity allows to minimize the energy amount required for magnetization reversal, and high magnetic saturation enables more reliable operation through the increase of the magnetic coupling between the magnets.

To ensure signal directionality within neighboring magnets, one side of every nanomagnet is irradiated with Ga^+ ions by a focused ion beam (FIB). Accelerated Ga^+ ions at high voltages locally destroy the PMA-inducing interfaces between the Co and Pt layers at the exposed area.[13,14] This irradiated area is the magnet's weakest spot and therefore determines the nucleation point for the magnetization reversal. Such spot is known as artificial nucleation center (ANC) and allows to make one magnet susceptible only to the neighboring magnets on one side. This ensures the required signal directionality in chains and arrays of field-coupled magnets.[15]

III. MAGNETIZATION REVERSAL IN NS-RANGE

Until now, pNML was mostly investigated in the μs-range. However, progressive scaling with better lithography enables clocking frequencies up to the targeted GHz-range. This allows to increase the computing possibilities of pNML-based systems. Therefore, it is highly important to investigate the magnetization reversal of the nanomagnets in the sub-100 ns-range. We have set the experiment to investigate the magnetization reversal of a single Co/Pt nanomagnet by applying the magnetic field pulses within a wide range of pulse widths. We have employed three different methods of field generations to cover the widest possible time range, which should provide the help of fitting the commonly used models to the data. For the longest pulses in ms-range an extremal electromagnetic coil was employed. To generate the pulses in the several μs-range an air core

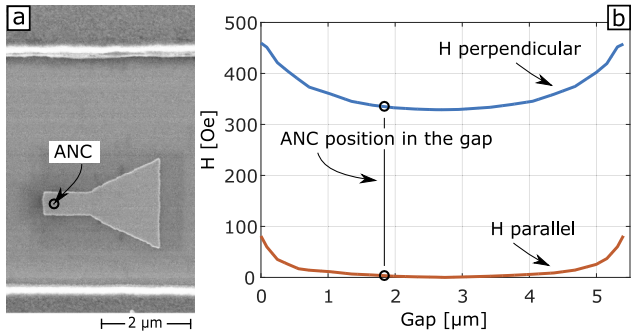

FIG. 1. (a) SEM image of a magnet with ANC in the gap of the on-chip field inductor; (b) The magnetic field amplitude in the gap between on-chip inductor fingers. The blue line shows the perpendicular, and the orange one presents the in-plane magnetic field amplitude components per 1 Ampere current.

micro-coil was used directly under the sample, furthermore, to cover the pulses from 1 μs to 20 ns, an on-chip inductor was fabricated.

A. Sample fabrication

The magnetic ultra thin multilayer film stack of $Ta_{3nm}/Pt_{3nm}/4x[Co_{0.8nm}/Pt_{1.5nm}]/Pt_4$ was RF magnetron sputtered with base pressure of 1.4×10^{-7} mBar, while Co was sputtered at 4 μbar and Pt at 2 μBar. The multilayer film was patterned by FIB-lithography and liftoff processes using a 40 nm PMMA resist, developed for 15 s and followed by Ti evaporation used as hard mask. The lift-off of Ti on the unexposed resist was achieved by submerging the sample into a heated NMP ultrasonic bath. The patterned Ti hard mask was transferred by argon ion beam etching to the ferromagnetic film stack to pattern the magnets. Finally, to determine the nucleation spot the FIB irradiation of 50 x 50 nm^2 area an one side of the magnet was performed. The ANC position can be seen in Fig. 1(a). A dose of 5×10^{13} Ions/cm^2 of Ga^+ ions by 50kV acceleration voltage was used and resulted in a coercive field reduction (H_c) of 52%. The switching field before irradiation was determined to 170 Oe and to 90 Oe after irradiation. To be able to apply short magnetic pulses the 500 nm thick Copper/Aluminum on-chip inductor was patterned and aligned by means of optical lithography.

Fig. 2 shows an image of the optical microscope and gives an overview of the sample layout. There are 4 on-chip inductors for magnetic field generation on the sample. The blue color exemplifies one of them. The inlet on the right side of Fig. 2 shows the investigated magnets in the 5.4μm gap between the fingers of the on-chip inductor. Fig. 1(a) shows the SEM image of a Co/Pt

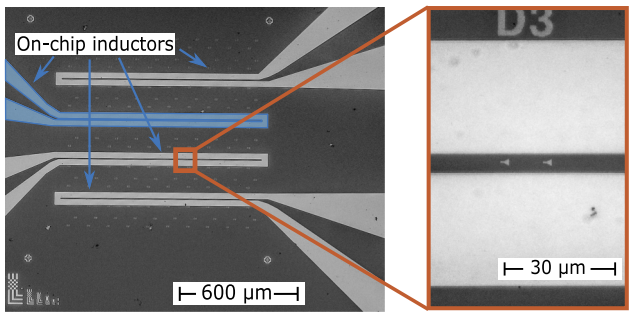

FIG. 2. An optical microscope image of the sample layout with four On-chip inductors. The Blue color exemplifies one of them. The inlet shows the gap between the fingers of one of the four on-chip inductors. In the 5.4 μm wide gap two Co/Pt magnets are placed.

magnet. The shape of a nanomagnet was designed in order to provide enough area for reliable laser Kerr-effect microscope measurements.

B. Measurements and Results

All presented data were obtained by measurements performed on one magnet in all ranges of applied pulse widths. In terms of reproducibility of this experiment also the neighboring magnets were investigated. The results showed the same important trend, therefore, it can be stated that extensive characterization of one magnet correctly represents magnetization reversal of nanomagnets, realized in the current Co/Pt pNML technology. The switching field is mostly determined by the ultra-thin film stack's quality, sputter parameters and the controlled anisotropy reduction by ion irradiation. The magnetic field amplitude generated by the on-chip inductor was simulated with FEMM[16] simulator. Fig. 1(b) shows the induced field across the whole gap of an on-chip inductor per 1 A injected current.[17] The FEMM simulation provides data, showing that 1 A current induces 338 Oe magnetic field in the area of the ANC.

Fig. 3 depicts the magnetization reversal probability at different field strengths for different pulse widths (from 1 μs to 20 ns). To obtain one curve N=100 field amplitude pulses were applied for every field step (ΔH = 11.12 Oe). After each pulse laser Kerr-effect microscope was used to evaluate the magnetization state of the magnet. Between pulses, the magnet was saturated with a magnetic field to the opposite direction. Then the amplitude was increased with 11.12 Oe step size until 100% switching probability was achieved. Fig. 3 shows that the measured switching probability curves for pulse lengths longer than 100 ns have very similar shape and slope. The corresponding field strength required for magnetization reversal only increases little with shorter pulse lengths. By contrast, the switching field amplitude increases rapidly for pulse lengths shorter than 100ns and the slope decreases significantly, leading to a wider corresponding switching field distribution. For pNML, a narrow distribution is preferred as it allows more reliable switching of the magnets and therefore leads to less error prone NML circuits and systems.[18]

The observed behavior above 100 ns can be modeled with the well known Arrhenius equation[5]:

$$P_{sw}(t_p, H_0) = 1 - \exp(-t_p/\tau(H_{eff})) \tag{1}$$

and

$$\tau(H_{eff}) = f_0^{-1} \exp\left(\frac{E_0(1 - \frac{H_{eff}}{H_0})^2}{k_b T}\right) \tag{2}$$

where t_p is the pulse time of the magnetic field, f_0 = 2GHz is reversal attempt frequency, k_b is the Boltzmann constant, and T is the temperature in Kelvin. The parameters E_0 and H_0 determine the magnetic reversal characteristics of the nanomagnet. E_0 is an energy barrier of the ANC at zero field. H_0 is the field required to change the magnetization direction of a magnet at zero temperature. Those constants can also be estimated analytically.[19]

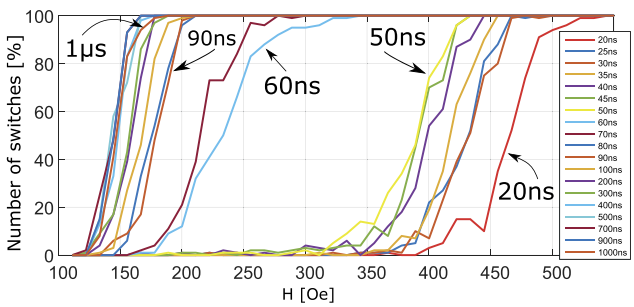

FIG. 3. Magnetization reversal characteristics measured by Laser-MOKE Microscope. Curves represent a magnetization state evaluation of one magnet applying each of depicted magnetic field's amplitudes for 100 times at one specified pulse width. The experiment was repeated for each pulse width depicted in different curve color.

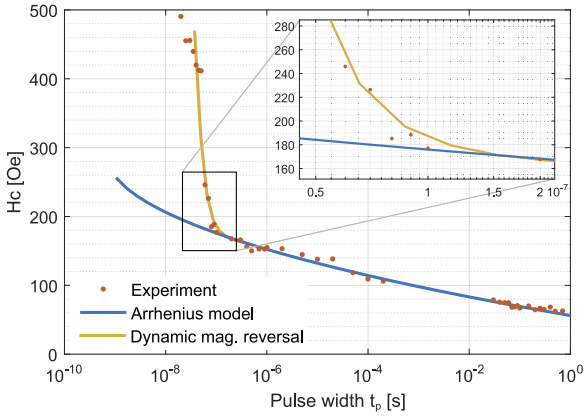

FIG. 4. Coercivity of the investigated magnet as function of the field pulse time (t_p). The orange dots show the measurement data while the blue solid line illustrates the commonly applied Sharrock equation to model the coercivity. The yellow solid line depicts the corrected model.

Resolving the Arrhenius equation to H_{eff} and setting $P_{sw} = 0.5$ results in the Sharrock formula[20]:

$$H_c(t_p) = H_0 \left[1 - \left(\frac{k_B T}{E_0} ln \left(\frac{f_0 t_p}{ln\,(2)} \right) \right)^{1/2} \right] \tag{3}$$

Fig. 4 depicts coercivity of a magnet as a function of time, the blue solid line depicts the Sharrock formula fitted to the experimental data which is visualized by orange dots. It can be observed that for the pulse widths shorter then $t_p < 100$ ns, the deviation from the standard Sharrock formula becomes unacceptable. To address this behavior the temperature independent τ term, instead of the one used in original Arrhenius equations (eq. (2)), was applied. For the shortest pulses the switching relies on "dynamic"temperature independent τ as follows:

$$\tau = \frac{1}{2(1-h)} \ln \left[\frac{h - 1 + 2\,\overline{n}_d}{(h+1)\overline{n}_d} \right] \tag{4}$$

with $h = H_{eff}/H_0$. The yellow solid line depicts the modified Arrhenius model visualized in Sharrock's representation. To fit the standard Sharrock formula $E_0 = 33.5/k_bT$, $H_0 = 300$ Oe and $f_0 = 2$ GHz are used. For the corrected Arrhenius model the following parameters were used to fit to the experimental data: $H_0 = 157.9, \overline{n}_d = 2.95$ and f_0 correction factor $f_{0corr} = 2.05 \cdot 10^6$. This provides an analytical model for the GHz clocked pNML.

IV. CONCLUSION

We observed that the experimental data fits very well to the commonly used Arrhenius model with a single parameter set above 100 ns pulse length. However, below 100 ns, a steep increase of the pulse amplitude for switching is observed and the deviation from the Arrhenius model becomes unacceptable. For short pulse times the model can be adjusted by the reversal time term for the dynamic switching field, which is only dependent on pulse amplitude, but not on temperature.[21] Fig. 4 compares the conventional Arrhenius model to the altered (temperature independent) Arrhenius model for short pulses ($t_p < 100$ ns). Both models were calibrated to the experiment in two different time regimes respectively. Steep increase of field amplitude required for magnetic switching, which also results in higher energy consumption. For this reason optimization of the multilayer film stack is needed to postpone the point where the change from conventional (thermally assisted) to dynamic magnetic reversal happens. The ability to analytically describe the magnetization reversal on short pulse time scales enables precise physical compact modeling of pNML in targeted GHz-range. This

is crucially important to ensure reliable operation in the targeted GHz-range as well as to explore and design new kinds of pNML circuits and architectures.

ACKNOWLEDGMENTS

The authors would like to thank the DFG (Grant Nr. SCHM 1478/9-2 and SCHM 1478/11-1) for financial support.

[1] B. Krzanich, "Intel chief raises doubts over moores law" (2015).
[2] "The International Technology Roadmap for Semiconductors (ITRS): Emerging Research Devices (ERD)" (2013).
[3] J. Hutchby, "The nanoelectronics roadmap," *Emerging Nanoelectronic Devices* (John Wiley & Sons Ltd, 2014), pp. 1–14.
[4] R. P. Cowburn and M. E. Welland, "Room temperature magnetic quantum cellular automata," Science **287**, 1466–1468 (2000).
[5] M. Becherer, J. Kiermaier, S. Breitkreutz, I. Eichwald, G. Žiemys, G. Csaba, and D. Schmitt-Landsiedel, "Towards on-chip clocking of perpendicular Nanomagnetic Logic," Solid-State Electronics **102**, 46–51 (2014).
[6] D. James, "Intel 14 nm generation tri-gate technical analysis reports" (2015).
[7] I. Eichwald, S. Breitkreutz, J. Kiermaier, G. Csaba, D. Schmitt-Landsiedel, and M. Becherer, "Signal crossing in perpendicular nanomagnetic logic," Journal of Applied Physics **115**, 17E510 (2014).
[8] I. Eichwald, S. Breitkreutz, G. Ziemys, G. Csaba, W. Porod, and M. Becherer, "Majority logic gate for 3D magnetic computing," Nanotechnology **25**, 335202 (2014).
[9] S. Breitkreutz, J. Kiermaier, I. Eichwald, X. Ju, G. Csaba, D. Schmitt-Landsiedel, and M. Becherer, "Majority Gate for Nanomagnetic Logic With Perpendicular Magnetic Anisotropy," IEEE Transactions on Magnetics **48**, 4336–4339 (2012).
[10] S. Breitkreutz, A. Fischer, S. Kaffah, S. Weigl, I. Eichwald, G. Ziemys, D. Schmitt-Landsiedel, and M. Becherer, "Time-dependent domain wall nucleation probability in field-coupled nanomagnets with perpendicular anisotropy," Journal of Applied Physics **117**, 17B503 (2015).
[11] H. Kurt, M. Venkatesan, and J. M. D. Coey, "Enhanced perpendicular magnetic anisotropy in Co/Ni multilayers with a thin seed layer," Journal of Applied Physics **108**, 073916 (2010).
[12] J. Sinha, M. Hayashi, A. J. Kellock, S. Fukami, M. Yamanouchi, H. Sato, S. Ikeda, S. Mitani, S.-h. Yang, S. S. P. Parkin, and H. Ohno, "Enhanced interface perpendicular magnetic anisotropy in Ta CoFeB MgO using nitrogen doped Ta underlayers," Applied Physics Letters **102**, 242405 (2013).
[13] J. H. Franken, M. Hoeijmakers, R. Lavrijsen, and H. J. M. Swagten, "Domain-wall pinning by local control of anisotropy in pt/co/pt strips," Journal of Physics: Condensed Matter **24**, 024216 (2012).
[14] C. Vieu, J. Gierak, H. Launois, T. Aign, P. Meyer, J. P. Jamet, J. Ferré, C. Chappert, T. Devolder, V. Mathet, and H. Bernas, "Modifications of magnetic properties of Pt/Co/Pt thin layers by focused gallium ion beam irradiation," Journal of Applied Physics **91**, 3103 (2002).
[15] S. Breitkreutz, J. Kiermaier, S. Vijay Karthik, G. Csaba, D. Schmitt-Landsiedel, and M. Becherer, "Controlled reversal of Co/Pt Dots for nanomagnetic logic applications," Journal of Applied Physics **111**, 07A715 (2012).
[16] D. Meeker, "Finite element method magnetics" (2010).
[17] The misalignment is taken in to the account and is assured the in plane competent of overall field is just 1% of perpendicular to the surface component.
[18] S. Breitkreutz, I. Eichwald, J. Kiermaier, A. Papp, G. Csaba, M. Niemier, W. Porod, D. Schmitt-Landsiedel, and M. Becherer, "1-Bit Full Adder in Perpendicular Nanomagnetic Logic using a Novel 5-Input Majority Gate," EPJ Web of Conferences **75**, 05001 (2014).
[19] A. Hubert and R. Schäfer, "Magnetic Domains" (Springer-Verlag Berlin Heidelberg, 1998)
[20] M. Sharrock and J. McKinney, "Kinetic effects in coercivity measurements," IEEE Transactions on Magnetics **17**, 3020–3022 (1981).
[21] V. L. Safonov and H. N. Bertram, ""Dynamic-thermal" reversal in a fine micromagnetic grain: Time dependence of coercivity," Journal of Applied Physics **87**, 5681 (2000).